STATICALLY-BALANCED DIRECT DRIVE ROBOT FOR COMPLIANCE CONTROL ANALYSIS

H. Kazerooni and S. Kim
Mechanical Engineering Department
University of Minnesota
Minneapolis, Minnesota

Abstract

A statically-balanced direct drive robot manipulator with new architecture is constructed at the University of Minnesota for stability analysis of Impedance Control [8,10,11]. This mechanism, using a four-bar-linkage, is designed without extra counterweights. As a result of the elimination of the gravity forces on the drive system, smaller actuators (and consequently smaller amplifiers) can be chosen. This guarantees an acceleration of 5g without overheating the motors. This mechanism results in closed-form solution for the inverse kinematics. The closed-form solutions for dynamics and inverse kinematics have been derived. High torque, low speed, brush-less AC synchronous motors are used to power the robot. The relatively "large" workspace of this configuration is suitable for manufacturing tasks. Graphite epoxy composite material is used for the construction of the robot links.

Introduction

A statically balanced direct drive arm, with a four-bar-linkage has been designed to compensate for some of the drawbacks of serial type [1,2,15] and parallelogram type [3,4,20] direct drive arms. Before describing the properties of this arm, some disadvantages and advantages of direct drive arms are discussed here:

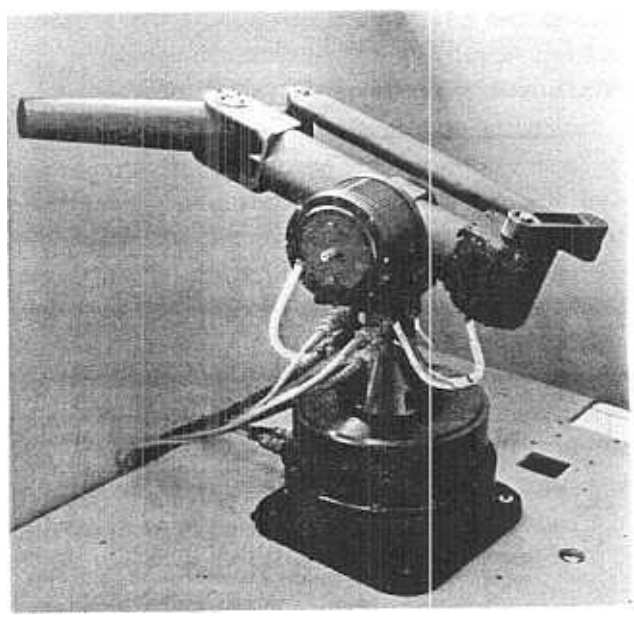

University of Minnesota Direct Drive Robot Manipulator

1. Speed. The maneuvering speed of the direct drive arms is not necessarily greater than the non-direct drive arms. The maximum achievable speed for a given architecture depends on the transmission ratio. The optimum transmission ratio is a function of the

inertia of the links. A simple example in appendix A shows that for a given architecture, a non-direct drive arm can be faster than a direct drive arm.

2. Static Payload. It is obvious that for a given set of motors, direct drive arms will have a lower static payload than non-direct drive arms. This is because of the inherent evident property of reducer transmission systems.

3. Overheating. Elimination of the transmission system causes the inertial force and the gravitational force of the links affect the motors directly. In other words, the motors "feel" the inertial and the gravitational forces without any reduction in size. The direct effect of the forces cause the motors to overheat in the direct drive arms. This overheating exists even in the static case when the arm is only under its static load.

4. Backlash and Friction. The direct drive arms are free from mechanical backlash and friction due to elimination of transmission systems. A small mechanical backlash in the transmission system would cause the gear teeth to wear faster. The high rate of wear in the gear would develop an even larger backlash. About 25% of the torque in non direct drive arms is used to overcome the friction[6].

5. Structural Stiffness. The structural stiffness of the direct drive arms is greater than the non-direct drive systems. About 80% of the total mechanical compliance in most non-direct drive industrial robots is caused by transmission systems[7,16]. The high structural stiffness allows for wide bandwidth control[18]. The low structural stiffness of non-direct drive arms, due to the existence of many mechanical elements in the transmission system, is a limiting factor on achievement of a relatively wide bandwidth control system.[10,11,12]

6. Performance and Control. Because of elimination of the transmission systems, and consequently backlash, the control and performance analysis of direct drive arms is more straightforward than the non-direct drive arms (not necessarily "easier").

7. Accuracy. The accuracy of direct drive arms is questionable. The lack of the transmission system eliminates cogging, backlash, and its corresponding limit cycle in the control system. On the other hand, the motor vibrations in the direct drive systems are directly transferred to the robot end point.

Motivation

The following scenario reveals the crucial needs for adaptive electronic compliance control (Impedance Control) [8,10,11] in manufacturing. Consider an assembly operation by a human worker. There are some parts on the table to be assembled. Each time the worker decides to reach the table and pick a part, she/he always encounters the table with non-zero speed. The worker assembles the parts with a non-zero speed also. The ability of the human hand to encounter an unknown and unstructured environment [9,19], with non-zero speed, allows for a higher speed of operation. This ability in human beings flags the existence of a compliance control mechanism in biological systems. This mechanism guarantees the "controllability" of contact forces in constrained maneuvering, in addition to high speed maneuvering in unconstrained environment. With the existing state of technology we do not have an integrated sensory robotic assembly system that can encounter an unstructured environment as a human worker can. No existing robotic assembly system is faster than a human hand. The compliancy in the human hand allows the worker to encounter the environment with non-zero speed. The above example does not imply that we choose to imitate human being factory level physiological/ psychological behavior as our model to develop an overall control system for manufacturing tasks such as assembly and finishing processes. We stated this example to show 1) A reliable and optimum solution for simple manufacturing tasks such as assembly does not exist; 2) the existence of an efficient, fast compliance control system in human beings that allows for superior and faster performance. We believe that Impedance Control is one of the key issues in the development of high speed manufacturing operations. A direct drive robot arm is constructed at the University of Minnesota to investigate the stability of the robot in high speed manufacturing tasks under Impedance Control methodology.

Architecture

The architecture of this arm is such that the gravity term is completely eliminated from the dynamic equations. This balanced mechanism is designed without adding any extra counterbalance

weights. The new features of this new design are as follows:

I. Since the motors are never affected by gravity, the static load will be zero. Hence no overheating results in the system in the static case.

II. Because of the elimination of the gravity terms, smaller motors with less stall torque (and consequently smaller amplifiers) can be chosen for a desired acceleration.

III. Because of the lack of gravity terms, higher accuracy can be achieved. This is true because the links have steady deflection due to constant gravity effect. This will give better accuracy and repeatability for fine manipulation tasks.

IV. As depicted in Figure 2, the architecture of this robot allows for a "large" workspace. The horizontal workspace of this robot is quite attractive from the stand point of manufacturing tasks such as assembly and deburring. Figure 1 shows the schematic diagram of the University of Minnesota direct drive arm. The arm has three degrees of freedom, all of which are articulated drive joints. Motor 1 powers the system about a vertical axis. Motor 2 pitches the entire four-bar-linkage while motor 3 is used to power the four-bar-linkage. Link 2 is directly connected to the shaft of motor 2. Figure 2 shows the top view and side view of the robot. The coordinate frame $X_iY_iZ_i$ has been assigned to link i of the robot for i=1,2,..,5. The center of coordinate frame $X_1Y_1Z_1$ corresponding to link 1 is located at point 0 as shown in figure 2. The center of the inertial global coordinate frame $X_0Y_0Z_0$ is also located at point 0 (The global coordinate frame is not shown in the figures). The joint angles are represented by θ_1, θ_2, and θ_3. θ_1 represents the rotation of link 1; coordinate frame $X_1Y_1Z_1$ coincides on global coordinate frame $X_0Y_0Z_0$ when $\theta_1=0$. θ_2 represents the pitch angle of the four-bar-linkage as shown in figure 2. θ_3 represents the angle between link 2 and link 3. Shown are the conditions under which the gravity terms are eliminated from the dynamic equations.

Figure 3 shows the four-bar-linkage with assigned coordinate frames. By inspection the conditions under which the vector of gravity passes through origin, 0, for all possible values of θ_1 and θ_3 are given by equations 1 and 2.

$$\{ m_3\bar{x}_3 - m_4L_5 - m_5\bar{x}_5 \} \sin\theta_3 = 0 \qquad (1)$$

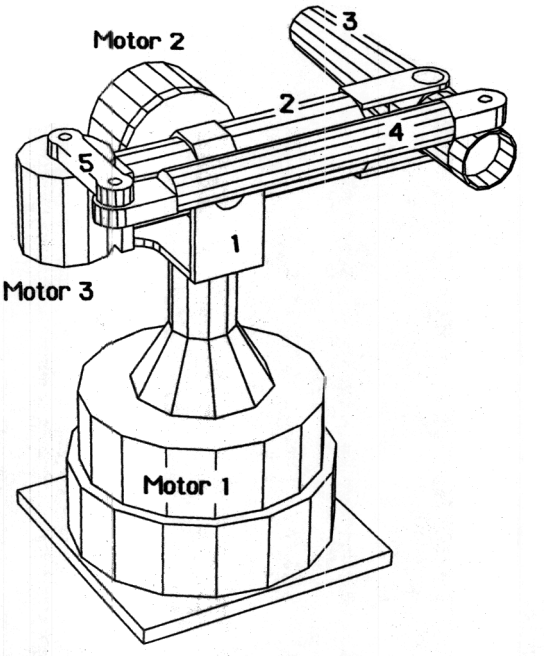

Figure 1: University of Minnesota Direct Drive Arm

$$g\,(mt_3 + m_5) - m_2\bar{x}_2 - m_3(L_2 - g) - m_4(\bar{x}_4 - g) - \{ m_3\bar{x}_3 - m_4L_5 - m_5\bar{x}_5 \} \cos\theta_3 = 0 \qquad (2)$$

where:

m_i = mass of each link,

L_i = length of each link,

$\bar{x}_i$ = the distance of center of mass from the origin of each coordinate frame,

mt_3 = mass of motor 3.

Conditions 1 and 2 result in:

$$m_3\bar{x}_3 - m_4L_5 - m_5\bar{x}_5 = 0 \qquad (3)$$

$$g\,(mt_3 + m_5) - m_2\bar{x}_2 - m_3(L_2 - g) - m_4(\bar{x}_4 - g) = 0 \qquad (4)$$

If equations 3 and 4 are satisfied, then the center of gravity of the four-bar-linkage passes through point 0 for all the possible configurations of the arm. Note that the gravity force still passes through 0 even if the plane of the four-bar-linkage is tilted by motor 2 for all values of θ_2.

Since at low speeds, AC torque motors do not tend to cog, we chose low speed, high torque, and brush-less AC synchronous motors to power the robot. Each motor consists of a ring shaped stator and a ring shaped permanent magnet rotor with a

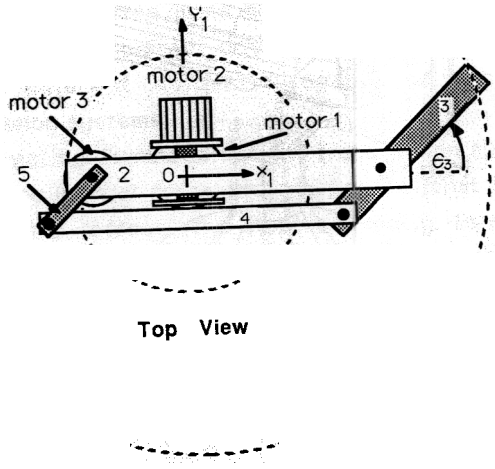

Top View

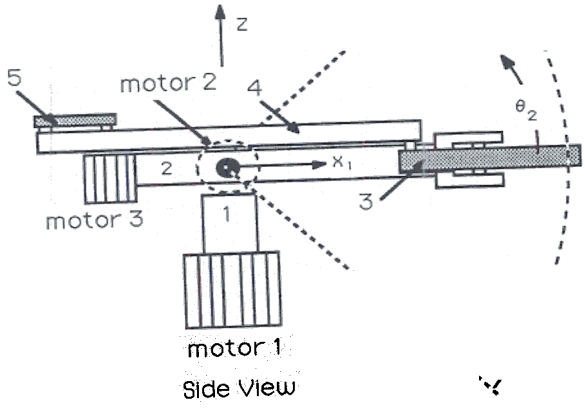

Side View

Figure 2: The Side View and Top View of the Robot

large number of poles. The rotor is made of rare earth magnetic material (Neodymium) bonded to a low carbon steel yoke with structural adhesive. The stator of the motor (with winding) is fixed to the housing for heat dissipation.

Forward Kinematics

The forward kinematic problem is to compute the position of the end point in the global coordinate frame $X_0Y_0Z_0$, given the joint angles, θ_1, θ_2, and θ_3. The joint coordinate relationship of the I coordinate frame relative to the i-1 coordinate frame in figure 4 can be represented by the homogeneous transformation matrix ${}^{i-1}T_i$ that follows the modified

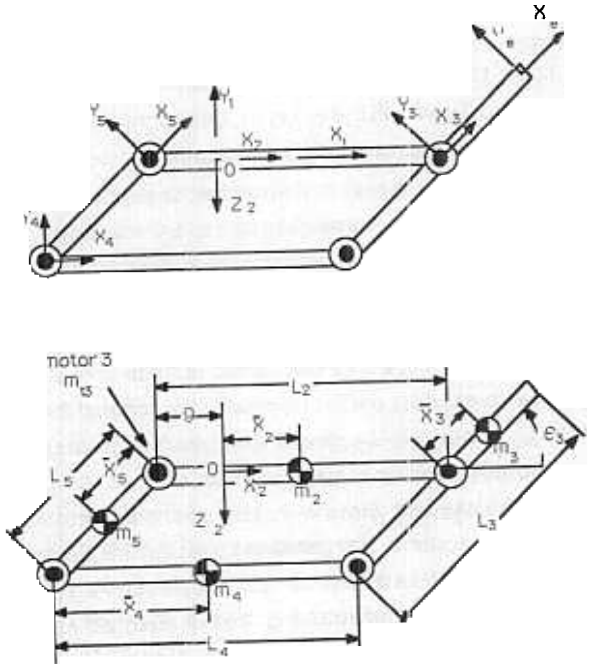

Figure 3: Four Bar Link Mechanism

Denavit Hartenberg notation. (6)

$$ {}^{i-1}T_i = \begin{bmatrix} C\theta_i & -S\theta_i & 0 & a_{i-1} \\ S\theta_i C\alpha_{i-1} & C\theta_i C\alpha_{i-1} & -S\alpha_{i-1} & -S\alpha_{i-1}d_i \\ S\theta_i S\alpha_{i-1} & C\theta_i S\alpha_{i-1} & C\alpha_{i-1} & C\alpha_{i-1}d_i \\ 0 & 0 & 0 & \end{bmatrix} \quad (5) $$

S and C refer to Sine and Cosine functions, and a_i, d_i, α_i and θ_i are link parameters. The link parameters of the arm are listed in table 1. Note that the coordinate frame $X_1Y_1Z_1$ coincides with the global coordinate frame, $X_0Y_0Z_0$, when θ_1 is zero.

The homogeneous transformation matrix, which describes the position and orientation of coordinate frame $X_eY_eZ_e$ with respect to the global coordinate frame $X_0Y_0Z_0$ is given by

$$ {}^{0}T_e \begin{bmatrix} C_1C_2C_3 - S_1S_3 & -C_1C_2S_3 - S_1C_3 & -C_1S_2 & (C_1C_2C_3 - S_1S_3)(L_3 - L_5) + C_1C_2(L_2 - g) \\ S_1C_2C_3 + C_1S_3 & -S_1C_2S_3 + C_1C_3 & -S_1S_2 & (S_1C_2C_3 + C_1S_3)(L_3 - L_5) + S_1C_2(L_2 - g) \\ S_2C_3 & -S_2S_3 & C_2 & S_2(L_2 - g) + S_2C_3(L_3 - L_5) \\ 0 & 0 & 0 & \end{bmatrix} \quad (6) $$

where $S_i = \sin(\theta_i)$, and $C_i = \cos(\theta_i)$

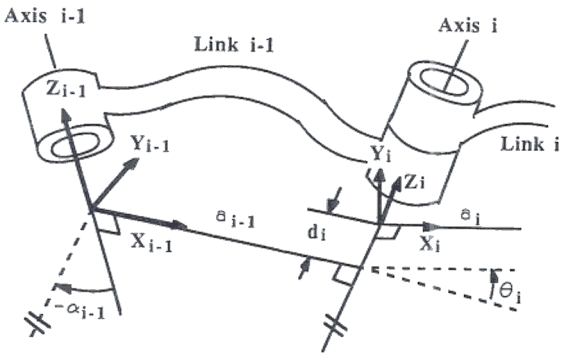

a_i = the distance from Z_i to Z_{i+1} measured along X_i;
α_i = the angle between Z_i and Z_{i+1} measured about X_i;
d_i = the distance from X_{i-1} to X_i measured along Z_i;
θ_i = the angle between X_{i-1} and X_i measured about Z_i;

Figure 4: Link Coordinates and Parameters

Table 1: Link parameters

Frame i	α_{i-1}	a_{i-1}	d_i	θ_i
$X_1Y_1Z_1$	0	0	0	θ_1
$X_2Y_2Z_2$	90°	0	0	θ_2
$X_3Y_3Z_3$	- 90°	$L_2 - g$	0	θ_3
$X_eY_eZ_e$	0	$L_3 - L_5$	0	0

Assume end point coordinate frame $X_eY_eZ_e$ has the same orientation as coordinate frame $X_3Y_3Z_3$

Inverse Kinematics

The inverse kinematic problem is to calculate the joint angles for a given end point position with respect to the global coordinate frame. The closed-form of inverse kinematics of the proposed arm derived using the standard method[6,17]. The end point position of the robot relative to the global coordinate frame is characterized by P_x, P_y, and P_z. The joint angles for the given end point position can be determined using the following equations

$$\theta_1 = \text{atan2}[P_y, P_x] - \text{atan2}[(L_3 - L_5)\sin\theta_3 \,/\sqrt{P_x^2 + P_y^2 - (L_3 - L_5)^2\sin^2\theta_3}] \quad (7)$$

$$\theta_2 = \sin^{-1}\left\{\frac{P_z}{[L_2 - g \quad \cos\theta_3}\right. \quad (8)$$

$$\theta_3 = \cos^{-1}\left\{\frac{P_x^2 + P_y^2 + P_z^2 - (L_2 - g)^2 - (L_3 - L_5)^2}{2[L_2 - g \quad (L_3 - L_5}\right. \quad (9)$$

Dynamics

The closed-form dynamic equations have been derived for the purpose of controller design. The dynamic behavior of the arm can be presented by the following equation (5,6)

$$M(\theta)\ddot{\theta} + CE(\theta)[\dot{\theta}^2] + CO(\theta)[\dot{\theta}\dot{\theta}] + G(\theta) = \tau \quad (10)$$

Where:

$\tau = [\tau_1\ \tau_2\ \tau_3]^T$ 3×1 vector of the motor torques,
$M(\theta)$ 3×3 position dependent symmetric positive definite inertia matrix,
$CE(\theta)$ 3×3 centrifugal coefficients matrix,
$CO(\theta)$ 3×3 Coriolis coefficients matrix,
$G(\theta)$ 3×1 vector of gravity force,
$\ddot{\theta} = [\ddot{\theta}_1\ \ddot{\theta}_2\ \ddot{\theta}_3]^T$
$[\dot{\theta}\dot{\theta}] = [\dot{\theta}_1\dot{\theta}_2 \quad \dot{\theta}_1\dot{\theta}_3 \quad \dot{\theta}_2\dot{\theta}_3]^T$
$[\dot{\theta}^2] = [\dot{\theta}_1^2 \quad \dot{\theta}_2^2 \quad \dot{\theta}_3^2]^T$

$$M(\theta) = \begin{pmatrix} M_{11} & M_{12} & M_{13} \\ M_{12} & M_{22} & 0 \\ M_{13} & 0 & M_{33} \end{pmatrix}, \quad CE(\theta) = \begin{pmatrix} 0 & CE_{12} & CE_{13} \\ CE_{21} & 0 & 0 \\ CE_{31} & CE_{32} & 0 \end{pmatrix}$$

$$CO(\theta) = \begin{matrix} CO_{11} & CO_{12} & CO_{13} \\ 0 & CO_{22} & CO_{23} \\ CO_{31} & 0 & 0 \end{matrix} \qquad G(\theta) = \begin{pmatrix} 0 \\ 0 \\ 0 \end{pmatrix}$$

$$M_{11} = I_{z1} + C_2^2[I_{e1} + I_{e6} + I_{e2} + 2C_3 I_{e3} + I_{y2} + m_2\bar{x}_2^2] + S_2^2[S_3^2 I_{e1} + I_{e5}] + C_3^2 I_{e4} + I_{x2})$$
$$M_{12} = S_2S_3[I_{e3} + C_3[I_{e1} + I_{e5} - I_{e4}]]$$
$$M_{13} = C_2[I_{e1} + I_{e6} + C_3 I_{e3}]$$
$$M_{22} = I_{z2} + m_2\bar{x}_2^2 + C_3^2[I_{e1} + I_{e5}] + S_3^2 I_{e4} + I_{e2} + 2C_3 I_{e3}$$
$$M_{33} = I_{e1} + I_{e6}$$

$$CE_{12} = C_2S_3[I_{e3} + C_3[I_{e1} + I_{e5} - I_{e4}]]$$
$$CE_{13} = -C_2S_3 I_{e3}$$
$$CE_{21} = S_2C_2[I_{y2} - I_{x2} + m_2\bar{x}_2^2 - S_3^2 I_{e5} + C_3^2[I_{e1} - I_{e4}] + I_{e2} + I_{e6} + 2C_3 I_{e3}$$
$$CE_{31} = S_3[C_2^2 I_{e3} - S_2^2 C_3[I_{e1} + I_{e5} - I_{e4}]]$$
$$CE_{32} = S_3[I_{e3} + C_3[I_{e1} + I_{e5} - I_{e4}]]$$

$$CO_{11} = -2CE_{21}$$
$$CO_{12} = -2CE_{31}$$
$$CO_{13} = -S_2[2S_3^2 I_{e1} + I_{e6} + \cos2\theta_3 \quad I_{e4} \quad I_{e5}]]$$
$$CO_{22} = S_2[2C_3^2 I_{e1} + I_{e6} + 2C_3 I_{e3} - \cos2\theta_3 [I_{e4} - I_{e5}]]$$
$$CO_{23} = -2CE_{32}$$

$$CO_{31} = -S_2[\, I_{e1} + \cos 2\theta_3\,(\, I_{e1} + I_{e5} - I_{e4}) + I_{e6} + 2C_3 I_{e3}]$$

where:

$I_{e1} = m_3\bar{x}_3^2 + m_4 L_5^2 + m_5\bar{x}_5^2$

$I_{e2} = m_3 (L_2 - g\,)^2 + m_4\,(\bar{x}_4 - g)^2 + m_5 g^2$

$I_{e3} = m_3\bar{x}_3(L_2 - g\,) - m_4\,(\bar{x}_4 - g)L_5 + m_5\bar{x}_5 g$

$I_{e4} = I_{x3} + I_{x4} + I_{x5}$

$I_{e5} = I_{y3} + I_{y4} + I_{y5}$

$I_{e6} = I_{z3} + I_{z4} + I_{z5}$

I_{xi}, I_{yi}, and I_{zi} are the mass moments of inertia relative to x, y, z axis at the center of mass of a link i. (motor 3 is a part of link 2). The gravity term, $G(\theta)$ becomes zero when equations 3, 4 are satisfied in the arm. This condition holds for all possible configurations. The values for various parameters are given in Appendix B.

Compliant Motion Control

The control method explained here is general and applies to all industrial and research robot manipulators. We take the time-domain nonlinear approach to arrive at the controller design methodology and its stability condition. The detailed controller design is given in references 13 and 14. A summary of the nonlinear modeling and the controller design is given here.

In general, manipulation consists of two categories. In the first category, the manipulator end-point is free to move in all directions. In the second, the manipulator end-point interacts mechanically with the environment. Most assembly operations and manufacturing tasks require mechanical interactions with the environment or with the object being manipulated, along with "fast" motion in free and unconstrained space. Therefore the object of the control task on this robot is to develop a control system such that the robot will be capable of "handling" both types of maneuvers without any hardware and software switches.

The design objective is to provide a stabilizing dynamic compensator for the robot manipulator such that the following design specifications are satisfied.

I. The robot end-point follows an input-command vector, r, when the robot manipulator is free to move.

II. The contact force, f, is a function of the input command vector, r, when the robot is in contact with the environment.

The first design specification allows for free manipulation when the robot is not constrained. If the robot encounters the environment, then according to the second design specification, the contact force will be a function of the input command vector. Thus, the system will not have a large and uncontrollable contact force. Note that r is an input command vector that is used for both unconstrained and constrained maneuverings. The end-point of the robot will follow r when the robot is unconstrained, while the contact force will be a function of r (preferably a linear function for some bounded frequency range of r) when the robot is constrained.

Note that the above notation does not imply a force control technique[22]. We are looking for a controller that guarantees the tracking of the input-command vector when the robot is not constrained, as well as the relation of the contact-force vector with the same input-command vector when the robot encounters an unknown environment.

The general form of the non-linear dynamic equations of a robot manipulator with positioning controller is given by two non-linear vector functions G and S in equation 11.

$$y = G(e) + S(d) \qquad (11)$$

where:

d = n×1 vector of the external force on the robot end-point

e = n×1 input trajectory vector

G = robot dynamics with positioning controller

r = n×1 input-command vector

S = robot manipulator stiffness

y = n×1 vector of the robot end-point position

e is the n×1 input trajectory vector that the robot manipulator accepts via its positioning controller. The fact that most manipulators have some kind of positioning controller is the motivation behind our approach. Also, a number of methodologies exist for the development of the robust positioning controllers for direct and non-direct drive robot manipulators. Using equation 10 and any controller

design method [21], one can always arrive at operator G such that it maps the input command vector, e, to the robot end-point position, y. The motion of the robot in response to imposed forces on the end-point is caused by either structural compliance in the robot or the positioning controller compliance. S represents this compliancy. Note that robot manipulators with positioning controllers are not infinitely stiff in response to external forces (also called disturbances).Even though the positioning controllers of robots are usually designed to follow the trajectory commandsand reject the disturbances, the robot end-point moves somewhat in response to imposed forces on the robot end-points. Although d and e affect the robot in a nonlinearfashion, equation 11 assumes that the motion of the robot end-point is a linear addition of both effects. No assumptions on the internal structure of G and S are made.

The dynamic behavior of the environment is given by mapping E in equation 12.

$$f=E(x) \qquad (12)$$

If one point of the environment is displaced as vector of x, then f is the required force to do such a task (Figure 5). E, represents the environment dynamics, while f and x are n×1 vector of the contact force and the environment deflection respectively. x_o is the initial location of the point of contact before

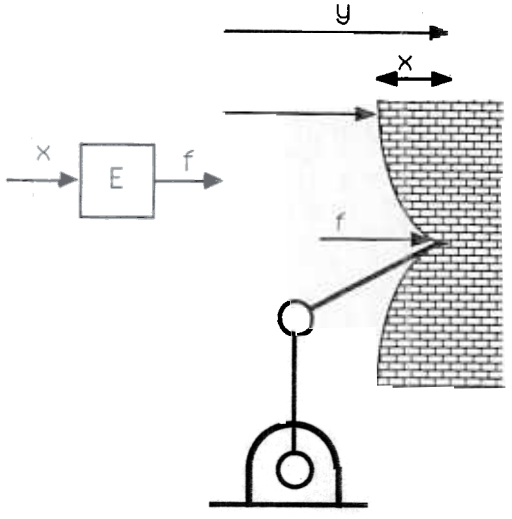

Figure 5: Environment and its Dynamics

deformation occurs and y is the robot end-point position ($x=y-x_o$). We assume G, S and E are stable operators in the L_p-sense [13,14]. The environment dynamics could be very "soft" or very "hard". We do not restrain ourselves to any geometry or structure for modeling the environment. We try to avoid the structured dynamic models such as first or second order transfer functions to represent the dynamic behavior of the environment. These models are not general and their corresponding simplified analysis consequently results in non-general conclusions.

The control architecture of Figure 6 shows how electronic compliancy is developed in the system. The input to the compensator, H is the contact force. The output of the compensator is subtracted from the input command vector, r. The discriminator block-diagram in Figure 6 shows that the environment and the robot may have uni-directional interaction. (such as pushing only). Note that when the robot is in interaction with the environment, $f=-d$ and $x=y-x_o$. There are two feedback loops in the system. The upper loop is the natural feedback loop. This loop shows how the contact force affects the robot in a natural way when the robot is in contact with the environment. The lower feedback loop is the controlled feedback loop.

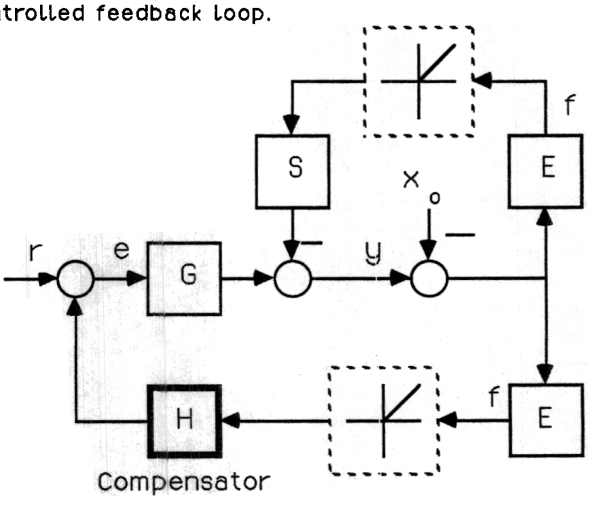

Figure 6: The Closed-Loop System

If the robot and the environment are not in contact, then the dynamic behavior of the system reduces to $y=G(r)$. When the robot and the environment are in contact, then the value of the contact force and the end-point position of robot are given by f and y where the following equations are true:

$$y=G(e)-S(f) \qquad (13)$$

$$f=E(x) \qquad (14)$$

$$e=r-H(f) \qquad (15)$$

We choose a class of compensators, H, to control the contact force with the input command r. This controller must also guarantee the stability of the closed-loop system shown in Figure 6. The input command vector, r, is used differently for the two categories of maneuverings; as an input trajectory command in unconstrained space and as a command to control of force in constrained space. We do not command any set-point for force as we do in admittance control. This method is called Impedance Control because it accepts a position vector as input and it reflects a force vector as output. There is no hardware or software switch in the control system when the robot travels from unconstrained space to constrained space. The feedback loop on the contact force closes naturally when the robot encounters the environment. V is introduced to represent the forward loop mapping from e to f. To guarantee the stability of the closed loop system, the L_p-norm of H must be less than the reciprocal of the "magnitude" (in the L_p-sense) of the mapping V in Figure 7.

$$\| H \| < \frac{\| e \|_P}{\| V(e) \|_P} \qquad (16)$$

A similar result has been derived for linear case (invariant nertia robot) using Nyquist stability criteria in reference 13.

$$\sigma_{max}[H] < \frac{}{\sigma_{max}[E(SE + I_n)^{-1}G]} \quad \text{for all } \omega \in (0,\infty)$$

The stability bound automatically leads to selection of the class of compensators, H.

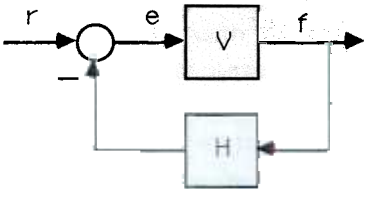

Figure 7: Manipulator and the Environment with Force Feedback Compensator, H (simplified version of Figure 6)

Summary

This paper presents some results of the on-going research project on statically-balanced direct drive arm at the University of Minnesota. The following features characterize this robot:

1. The statically-balanced mechanism without counter weights allows for selection of smaller actuators. Since in static or quasi-static operations, no load is on the actuators, therefore the overheating of the previous direct drive robots will be alleviated.
2. The robot links are made of graphite-epoxy composite materials to give more structural stiffness and less mass. The high structural stiffness and low mass of the links allow for the wide bandwidth of the control system.
3. Electronic compliancy (impedance control) has been considered for control of the robot. The object of the control task is to develop a control system such that, this robot will be capable of maneuvering in both constrained and unconstrained environments.

Appendix A

A simple example is given here to show the that transmission system does not necessarily results in lower speed for the output shaft. Consider the following system:

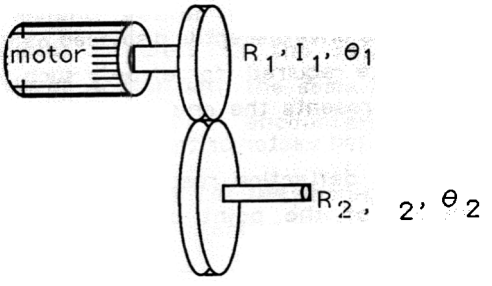

The dynamic equation describing the behavior of the system can be represented as:

$$\ddot{\theta}_2 = \frac{T}{(n\, I_1 + I_2/n)}$$

where (I_1, R_1, θ_1) and (I_2, R_2, θ_2) represent the moments of inertia, radius and angle of each gear $(n = R_2/R_1)$. T is the motor torque. It is clear that the maximum acceleration will happen when n is chosen as:

$$n = \sqrt{I_2 / I_1}$$

Appendix B

The uncertainty about the following parameters is about %10.

Link i	Length (cm)	$\bar{X}_i$ (cm)	Mass (kg)	Inertia (kg-cm^2 I_{xi}	I_{yi}	I_{zi}
				-	-	1.752
2	60.33	-11.17*	13.886*	0.421*	3.7805*	3.7805*
3	53.34	15.70	3.206	0.0397	0.4796	0.4796
4	60.33	30.16	2.924	0.0207	1.3253	0.0
5	15.24	7.62	0.758	0.0016	0.0694	0.0694
6	22.23	-	-	-	-	-

* In calculation of these values, we assume motor 3 is a part of link 2. For example 13.886kg in the above table includes mass of link 2 (4.626kg) and mass of motor 3 (9.26kg). The "height" of the robot, from the base to the origin of the $X_1Y_1Z_1$, is 62.992 cm (24.8 inch).

References

Asada, H., Kanade, T., "Design of Direct Drive Drive Mechanical arms", ASME Journal of Vibration, Acoustics, Stress, and Reliability in Design, vol. 105, July 1983, pp. 312 - 316

Asada, H., Kanade, K. and Takeyama, I., "A Direct-Drive Manipulator development of a High Speed Manipulator", in Brain, R. (compile), Development in Robotics 1984, Anchor Press, England, 1983, pp 217-226.

3 Asada, H., Youcef-Toumi, K. and Ramirez, R., "M.I.T. Direct Drive arm Project", Conference proceedings of Robots 8, vol.2, Robotics International of SME, 1984, pp 16-10 - 16-21.

4 Asada, H. and Youcef-Toumi, K., " Analysis and Design of a Direct Drive Arm with a Five-Bar-Link Parallel Drive Mechanism ", ASME Journal of Dynamic Systems, Measurement and Control, vol. 106 No. 3, 1984, pp 225-230.

5 Asada, H. and Slotine, J.-J.E., "Robot Analysis and Control", John Wiley and Sons, 1986.

6 Craig, J. J., "Introduction to Robotics: Mechanics and Control, Addison-Wesley, Reading, Mass 1986.

Forres-Barlach, M. G. and Babcock, S. M., "Inverse Dynamics Position Control of a Compliant Manipulator", IEEE International Conference on Robotics and Automation, 1986.

Hogan, N., " Impedanc1: Theory, Part 2: Implementation, Part 3: Application", ASME Journal of Dynamic Systems, Measurement, and Control, 1985.

9. Houk, J. C., Rymer, W. Z., "Neural Control of Muscle Length and Tension", in Handbook of Physiology - The Nervous System II, pp257-323.
10. Kazerooni, H., Sheridan, T., B., Houpt, P. K., "Fundamentals of Robust Compliant Motion for Robot Manipulators" , IEEE Journal on Robotics and Automation, vol. 2, NO. 2, June 1986.
11. Kazerooni, H., Houpt, P. K., Sheridan, T., B., " Design Method for Robust Compliant Motion for Robot Manipulators", IEEE Journal on Robotics and Automation, vol. 2, NO. 2, June 1986.
12. Kazerooni, H., Houpt, P. K.," On the Loop Transfer Recovery", International Journal of Control, vol. 43, NO. 3, March 1986.
13. Kazerooni, H., "Robust Non-Linear Impedance Control", In proceedings of the IEEE International Conference on Robotics and Automation, Raleigh, North Carolina, April 1987.
14. Kazerooni, H., Balkovicius, J., Guo, J., "Compliant Motion Control for Robot Manipulators, Input Output Approach", In proceeding of the American Control Conference, June 1987, Minneapolis.
15. Kuwahara, H., One, Y., Nikaido, M. and Matsumoto, T.," A Precision Direct Drive Robot Arm", Proceedings 85 American Control Conference, 1985, pp 722-727.
16. Mahalingam, S. and Sharan, A. M. "The Optimal Balancing of the Robotic Manipulators", IEEE 1986 International Conference on Robotics and Automation, vol. 2, April. 1986, pp 828-835.
17. Paul, R. P., Robot Manipulators: Mathematics, Programming, and Control", MIT press, Cambridge, Mass, 1981.
18. Rivin, E.I., "Effective Rigidity of Robot Structures: Analysis and Enhancement", Proceedings of 85 American Control Conference, 1985, pp 381-382.
19. Stein, R. B., "What muscle variable(s) does the Nervous System Control in Limb Movement?", The Behavioral and Brain Sciences, 1982, pp. 535-577.
20. Takase, K., Hasegawa, T. and Suehiro, T., "Design and Control of a Direct Drive Manipulator", Proceedings of the International Symposium on Design and Synthesis, Tokyo, Japan, July 1984,pp 347-352.
21. Vidyasagar, M., Spong, M. W., "Robust nonlinear Control of Robot Manipulators", IEEE Conference on Decision and Control", December 1985.
22. Whitney, D. E., "Force-Feedback Control of Manipulator Fine Motions", ASME Journal of Dynamic Systems, Measurement, and Control :91-97, June, 1977.